

High-order Treatment of Junctions and Edge Singularities with the Locally-corrected Nyström Method

M. M. Bibby and A. F. Peterson

School of Electrical and Computer Engineering
Georgia Institute of Technology, Atlanta, GA, 30332-0250, USA
mbibby@ece.gatech.edu, peterson@ece.gatech.edu

Abstract—High order techniques are known to be effective for the electromagnetic analysis of smooth structures. In the following, high order representations developed for the current density at edges and junctions are incorporated into the locally-corrected Nyström method. Conducting structures used for purposes of illustration include a strip, a structure with three fins and a junction, and a hexagonal cylinder. Results suggest that the accuracy of the numerical results obtained with the new approach is comparable to that obtained for problems with smooth surfaces.

Index Terms—Edge singularities, high order representations, junction conditions, and singular basis functions.

I. INTRODUCTION

High-order numerical techniques are those in which the representation of the primary unknown is usually in terms of a polynomial of degree $p \geq 2$ and the convergence rate of the solution is much faster than $O(h^2)$, where h is the nominal cell dimension. These techniques have been effective for obtaining high accuracy and rapid convergence in numerical solutions of integral equations for electromagnetics [1-3], at least for smooth structures. Recent publications report a method-of-moments (MoM) procedure that permits similar improvement in accuracy for 2D structures with edges where the current density or charge density exhibits a singularity [4-5]. That approach used a high order representation containing appropriate fractional powers of polynomial terms in the cells adjacent to an edge where a current singularity occurs. For those structures, the rate of decrease in

the error improves with reduced cell sizes as either the basis function or the representation order increases. In the following, a similar procedure is incorporated into the locally-corrected Nyström (LCN) method.

In Nyström approaches, the representation of the unknown quantity is provided indirectly by a quadrature rule. Degrees of freedom such as the fractional polynomial powers needed for edge singularities can be obtained by the use of quadrature rules specifically created to incorporate those terms. Extensions of the LCN for the special case of a knife-edge singularity were previously proposed by Gedney et al. [6], Gedney [7], and Tong and Chew [8]. The present work differs in that it is applicable to corners of any angle, and it incorporates quadrature rules that can integrate multiple singular terms at each edge in order to achieve true high order behavior. Results indicate that as the order of the representation for the current density increases, the accuracy of the solution improves at the same rates observed for smooth geometries.

The LCN method is usually implemented without imposing any condition on the continuity of the current density representation across cell boundaries. Consequently, one might question the extent to which the LCN results near a junction between three or more cells (such as the “fin” structure in Fig. 1) satisfy Kirchhoff’s current law (KCL). In fact, high order behavior is not obtained unless the current density is modeled to the same accuracy level everywhere. In the following, an approach similar to that used at edges is applied to model the current density in cells adjacent to junctions.

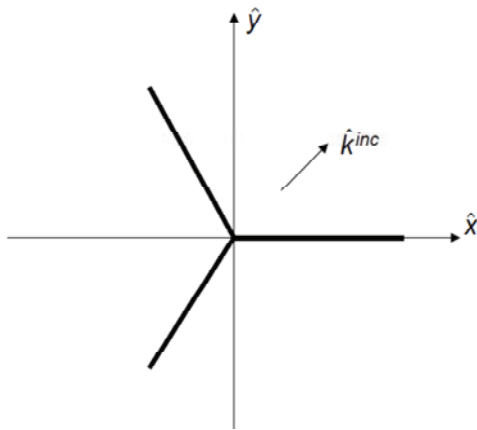


Fig. 1. A perfectly conducting structure, consisting of 3 fins and a junction. The structure is infinite in the z direction, and the angle between adjacent fins is 120 degrees.

A preliminary description of the treatment of edges, with examples that differ from those presented below, was given in [9] and [10]. The treatment of junctions using the MoM and LCN was briefly discussed in [11]. An extensive list of references on the treatment of edge singularities was included in [4]; a similarly extensive list of references on the LCN approach may be found in [10].

II. SINGULAR REPRESENTATION FOR EDGES

A solution for the surface current density induced on an infinite wedge is developed in [12]. Based on those results, a general asymptotic expression for the current density as a function of ρ on the face of a wedge (Fig. 2) with interior angle α , near the tip ($\rho = 0$), can be written for the transverse magnetic (TM)-to- z case as,

$$J_z : \sum_{m=0}^{\infty} \sum_{n=1}^{\infty} c_{mn} \rho^{2m+\nu_n-1} \quad (1)$$

where a cylindrical coordinate system (ρ, ϕ, z) is employed. In equation (1),

$$\nu_n = \frac{n\pi}{(2\pi - \alpha)}, \quad n = 1, 2, 3, \dots \quad (2)$$

A similar expression for the transverse electric (TE)-to- z case is,

$$J_\rho : \sum_{m=0}^{\infty} \sum_{n=0}^{\infty} d_{mn} \rho^{2m+\nu_n} \quad (3)$$

where ν_n is defined as,

$$\nu_n = \frac{n\pi}{(2\pi - \alpha)}, \quad n = 0, 1, 2, \dots \quad (4)$$

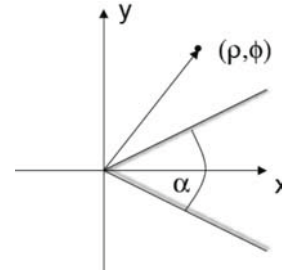


Fig. 2. Wedge tip geometry.

To properly model singular edge currents in the context of the MoM, reference [4] proposed basis functions for use in cells adjacent to geometric corners. For cells that are not adjacent to a corner of the contour, a Legendre expansion of order q is employed. In the corner cells, the representation is augmented by including some number of terms with non-integer exponents from equations (1) or (3). Empirical evidence [4-5] suggests that the singular behavior can be confined to single edge cells if those cells are sufficiently large (perhaps a quarter wavelength in dimension). Since the singular representation in equations (1) or (3) is sufficient only in a small neighborhood of the edge, for large cells it is necessary to mix regular (polynomial) terms with the singular terms to properly represent currents throughout that cell. The authors concluded in [5] that if q polynomial terms are used in non-corner cells, the local error near the corner can be reduced to the level of the error produced in the cells away from the corner by combining q regular terms and q singular terms in corner cells that are twice the size of the non-corner cells. The latter approach is used in the following to create quadrature rules that can be used within a Nyström discretization, and also as the basis functions used for local corrections.

Examples to follow will employ structures with interior wedge angles of 0 and 120 degrees. From equation (1), the transverse-magnetic-to- z (TM) current near 0 degree angle involves exponents, in increasing order, of

$$\left\{ \frac{-1}{2}, 0, \frac{1}{2}, 1, \frac{3}{2}, 2, \frac{5}{2}, 3, \dots \right\}. \quad (5)$$

For the transverse-electric-to- z (TE) case, the set of exponents for a 0 degree angle obtained from equation (3) is

$$\left\{0, \frac{1}{2}, 1, \frac{3}{2}, 2, \frac{5}{2}, 3, \frac{7}{2}, \dots\right\}. \quad (6)$$

For the 120 degree case, TM currents require the exponents

$$\left\{\frac{-1}{4}, \frac{1}{2}, \frac{5}{4}, \frac{7}{4}, 2, \frac{5}{2}, \frac{11}{4}, \frac{13}{4}, \dots\right\}, \quad (7)$$

while TE currents require

$$\left\{0, \frac{3}{4}, \frac{3}{2}, 2, \frac{9}{4}, \frac{11}{4}, 3, \frac{7}{2}, \dots\right\}. \quad (8)$$

However, using the approach of [5], the representation for currents at an edge incorporates an equal number of singular terms and regular terms. When integer exponents occur in the series, and duplicate the regular terms in the basis set, we incorporate additional fractional exponents from the series in their place. Table I summarizes the suggested degrees of freedom for a 0 degree TM corner (a knife edge).

Table I: Exponents of the degrees of freedom used for a given order, for cells near a 0 degree corner (TM case). The corner cells involve twice as many degrees of freedom as the other cells, but are to be twice as large.

Order of representation q	Exponents used in non-corner cells	Exponents used in corner cells
1	0	$-1/2, 0$
2	0, 1	$-1/2, 0, 1/2, 1$
3	0, 1, 2	$-1/2, 0, 1/2, 1, 3/2, 2$
4	0, 1, 2, 3	$-1/2, 0, 1/2, 1, 3/2, 2, 5/2, 3$
5	0, 1, 2, 3, 4	$-1/2, 0, 1/2, 1, 3/2, 2, 5/2, 3, 7/2, 4$

Terms with the exponents in Table I are used to construct a hierarchical basis set as described in [4] and [10]. As an example, the “order-2” representations in the end cells for the 0 degree TM corner is obtained using the 4 functions

$$\left\{u - \frac{3}{2}u^{1/2} + \frac{3}{5} - \frac{1}{20}u^{-1/2}, u - \frac{4}{3}u^{1/2} + \frac{2}{5}, u - \frac{5}{6}u^{1/2}, u\right\}, \quad (9)$$

where a local coordinate $0 \leq u \leq 1$ is employed with $u = 0$ at the corner, and a basic Gram-Schmidt procedure is used to produce an

orthogonal set. (Since the $u^{-1/2}$ term cannot be integrated with itself, here basis functions incorporating the four terms are orthogonalized in the reverse order they appear in equation (5) to produce the set of equation (9). In the non-edge cells, an order-2 representation is obtained using the constant and linear Legendre polynomials,

$$\{1, 2u - 1\} \quad (10)$$

to represent the currents.

III. LCN IMPLEMENTATION

The LCN approach was proposed in [1] and is described in many publications, including [10], so we omit a review of the technique. Reference [10] also describes the details of how we treat the electric-field integral equation (EFIE) and magnetic field integral equation (MFIE), including the Green’s function singularities.

Two important aspects of an LCN approach necessary to implement the singular representation described above are a set of basis functions that can be used to “locally correct” the kernel of the integral operator when the sources reside in a cell containing a corner singularity, and a family of quadrature rules that can integrate the singular functions to high accuracy. The basis functions are obtained by combining the degrees of freedom associated with a particular wedge angle with polynomials, and orthogonalizing those terms using a Gram-Schmidt process, as described above for a 0 degree angle and discussed in [4] and [10] in more generality. Quadrature rules that can integrate the singular functions are usually not readily available, and for this work are synthesized from an expanded set of appropriate degrees of freedom, using a procedure similar to that of [13], which is also reviewed and explained in [10]. Several of these rules are provided below. Since a q -point quadrature rule can exactly integrate $2q$ independent terms, additional degrees of freedom from the family of terms for the relevant corner angle were employed in the generation of the quadrature rules. As in the non-singular case, when the quadrature rules are related to the basis functions in this manner, the accuracy of the overall LCN analysis will be limited by the basis functions used within the local correction procedure, and not by the quadrature rules.

The region over which the basis functions described above are used to “locally correct” the

singular kernel is the *local correction footprint*. In this work, local corrections are used whenever the observer or test point is within 0.15λ of any part of the source cell, where λ denotes the wavelength. Otherwise, the actual Green's function is sampled in accordance with the classical Nyström procedure. The 0.15λ footprint was selected after extensive numerical experiments. A more sophisticated scheme would adapt the size of the local correction footprint as needed to maintain a smooth transition between the synthetic and actual kernels.

To demonstrate the accuracy of the results that follow, we solve a 2:1 over-determined system of equations using a least-square algorithm [2], and calculate the normalized residual error (*NRE*) for the result from the residual of the over-determined system, as originally suggested by Bunch and Grow [14-15]. The *NRE* is defined for the TM-to-z electric-field integral equation (EFIE) on a perfectly conducting target as in [2],

$$NRE = \frac{\sqrt{\int |E_z^{inc} + E_z^s|^2 dt}}{\sqrt{\int |E_z^{inc}|_{\max}^2 dt}} \cong \frac{\sqrt{\sum_{i=1}^{N_p} w_i |E_z^{inc}(t_i) + E_z^s(t_i)|^2}}{|E_z^{inc}|_{\max} \sqrt{\sum_{i=1}^{N_p} w_i}} \quad (11)$$

where $\{t_i\}$ and $\{w_i\}$ denote Gauss-Legendre quadrature nodes and weights. N_{tp} is the total number of points included in the measure. For a global measure of *NRE*, N_{tp} is the total number of test points on the target. Alternatively, the *NRE* can be determined on a cell-by-cell basis; in that case equation (11) is computed for each cell with N_{tp} equal to the number of test points within that cell. As noted above, the number of test points in a corner cell is twice the number of test points in other cells not adjacent to a corner. For the MFIE or the transverse-electric (TE) EFIE, equation (11) is modified in an obvious way to implement the appropriate residual.

LCN unknowns are the samples of current density at the nodes of a quadrature rule. Since the integral equation is enforced at twice as many match points as unknowns, the test points are not the nodes defining the unknown samples. In this study, test points are the nodes of a Gauss-Legendre rule with the appropriate number of points, even in the end cells where a different quadrature rule is used to define the LCN

discretization. Appendix A describes an interpolation approach used to distribute the weights associated with the identity operator in the MFIE.

The rate at which the global *NRE* decreases as a function of cell size or number of unknowns can be used to judge the extent to which high order behavior is exhibited by the results. Consider two results, the first yielding NRE_1 with N_1 unknowns, and the second exhibiting NRE_2 with N_2 unknowns. The incremental slope of the associated error curve may be obtained from successive results using,

$$Slope_q = \frac{\log_{10}(NRE_2) - \log_{10}(NRE_1)}{\log_{10}(N_2) - \log_{10}(N_1)} \quad (12)$$

where the subscript serves as a reminder that the expansions are of order q . For scatterers with smooth surfaces [2], and targets with edges treated by the MoM approaches of [4-5], values of equation (12) often approximate integers as N increases. Similar behavior is observed with the LCN results.

We use an over-determined system of equations to compute the *NRE* and its slope and estimate the accuracy of a result. If the error estimate is not needed, LCN results can be obtained more efficiently with square systems of equations [10].

IV. EXAMPLE: SCATTERING FROM A CONDUCTING STRIP

To illustrate the approach, consider the scattering of a uniform TM plane wave from a flat, perfectly conducting strip with width of 7 wavelengths. The numerical solution is obtained by an application of the LCN approach to the EFIE. Gauss-Legendre quadrature rules are used within the LCN process for interior cells, while the special rules generated for knife-edge corners ($\alpha = 0$) are used in end cells. These quadrature rules for $q = 1-3$ are given in [10]. End cells are twice the dimension of other cells and use twice as many degrees of freedom (special quadrature rules for Nyström sampling and a number of singular terms equal to the number of regular terms in the functions used for the local corrections).

A high accuracy reference solution for the induced current J_z^{exact} on a conducting strip can be obtained in terms of an eigenfunction series of Mathieu functions [16]. To assess the accuracy of

the current density, Fig. 3 shows the error as a function of position on a strip modeled with 26 cells for two cases (the results are actually the superposition of the currents on either side of the strip). In the first case (the upper plots in Fig. 3), the end cell discretizations are obtained from the conventional LCN quadrature (Gauss-Legendre) rules, with the local correction provided by Legendre polynomial functions. In other words, no special edge treatment is applied. In the second case, the representation in the end cells is provided using quadrature rules that can integrate the mixture of exponents appearing in equation (5), and the local corrections are obtained using functions such as those in equation (9).

Figure 3 shows that if the conventional LCN representation is used in the end cells, there is no significant improvement in the results beyond order $q = 2$. However, when the singular representation is used in the end cells, there is a continuous improvement in the accuracy of the results as q increases, and the average error has improved by a factor of 10^{-9} for $q = 8$. We define the global normalized error in the current density (NEJ) as,

$$NEJ = \frac{\|J_z^{exact} - J_z^{num}\|}{|2\hat{n} \times \vec{H}^{inc}|_{\max}} = \frac{\sqrt{\frac{1}{N_p} \sum_{i=1}^{N_p} w_i |J_z^{exact}(t_i) - J_z^{num}(t_i)|^2}}{|2\hat{n} \times \vec{H}^{inc}|_{\max}} \quad (13)$$

where $\{t_i\}$ and $\{w_i\}$ denote Gauss-Legendre quadrature nodes and weights. Figure 4 shows the global NEJ as a function of the number of unknowns and the order q . As expected for higher order representations, these curves decrease with a steeper slope as q increases, despite the singularities at the strip ends. Although the slopes become somewhat erratic for higher values of q , they appear to approach integer values for lower q values and generally decrease as q increases.

Figure 5 shows results for the same strip when illuminated by a normally-incident TE wave, obtained from the LCN solution of the EFIE. The singular representations employed for the TE polarization are based on the exponents in equation (6), and do not include the $u^{-1/2}$ term used for the TM case. The basis functions and quadrature rules may be found in [10] up to $q = 3$. Although the edge singularity is weaker in the TE case and the current density is bounded, a polynomial representation cannot reduce the error

by more than a factor of 10^{-2} . However, the singular expansions facilitate a continuous improvement as the order increases, and reduce the average error by 10^{-8} for $q = 8$.

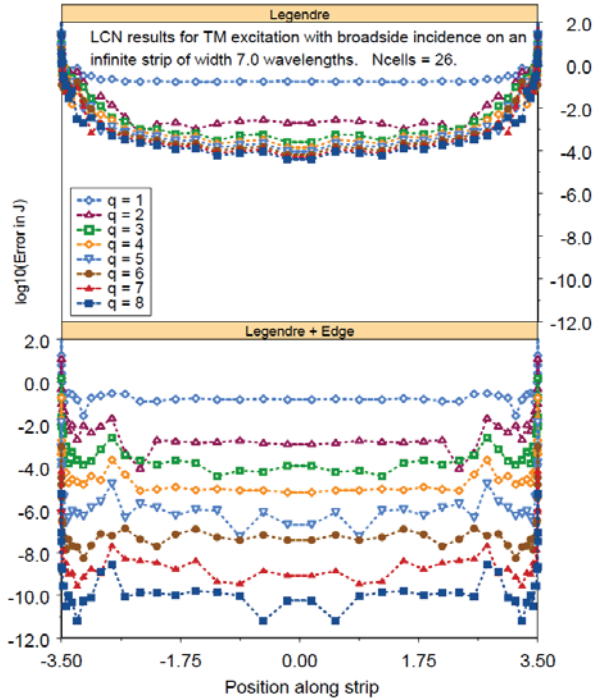


Fig. 3. Error in the current density as a function of position and order q , for a perfectly conducting 71 strip illuminated by a normally-incident TM plane wave. 26 cells are used to model the strip, with the end cells twice as large as the others. The upper figure shows the error when the end cells are treated with the same representation used in other cells; the lower figure shows the error when the singular representation is used in the end cells.

V. EXAMPLE: SCATTERING FROM A CONDUCTING 3-FIN STRUCTURE

Figure 1 shows a “3-fin” structure consisting of three perfectly conducting strips connected at the origin. For TE excitation, current is expected to flow across the junction between the strips. Since the LCN representation does not impose explicit current continuity between junctions, this structure provides a test bed for the satisfaction of Kirchhoff’s current law at the junction. In fact, both the open ends of the strips and the junction ends of the strips must be treated specially to obtain high order accuracy in this case. The 3-fin will be treated using the EFIE.

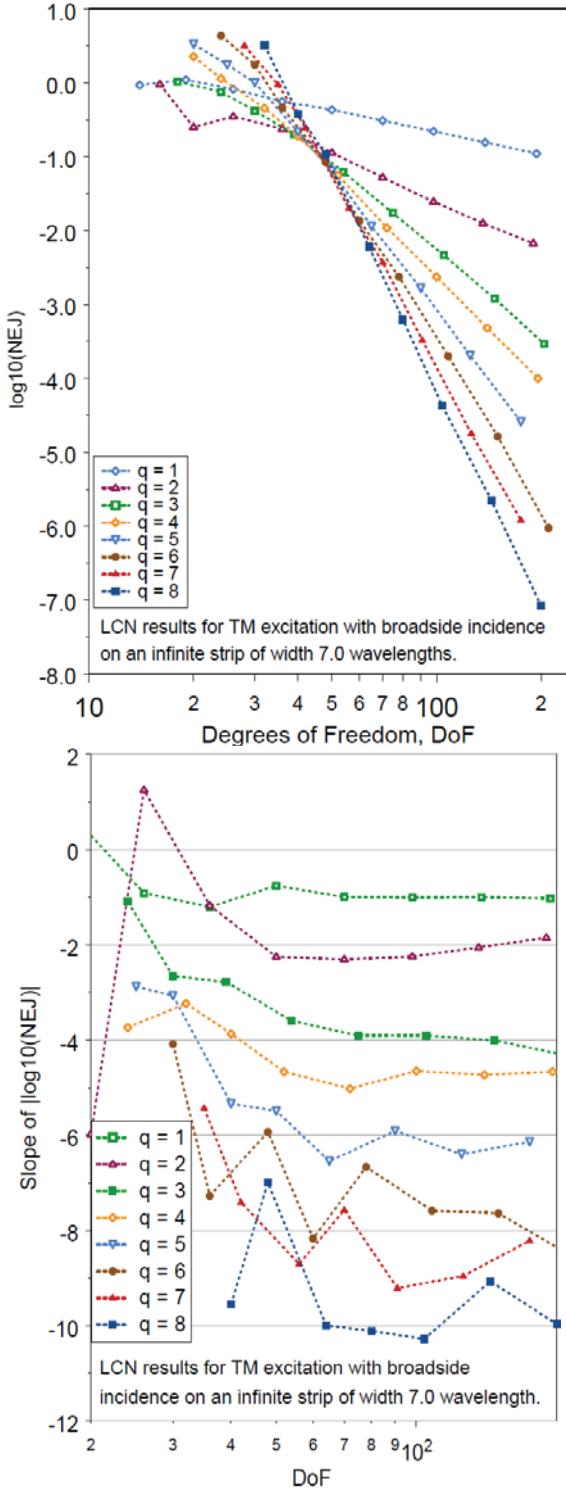


Fig. 4. (a) Global normalized error in the current density, NEJ , as a function of degrees of freedom and representation order q , for a perfectly conducting 7λ strip illuminated by a normally-incident plane TM wave and (b) slopes of the NEJ curves in (a).

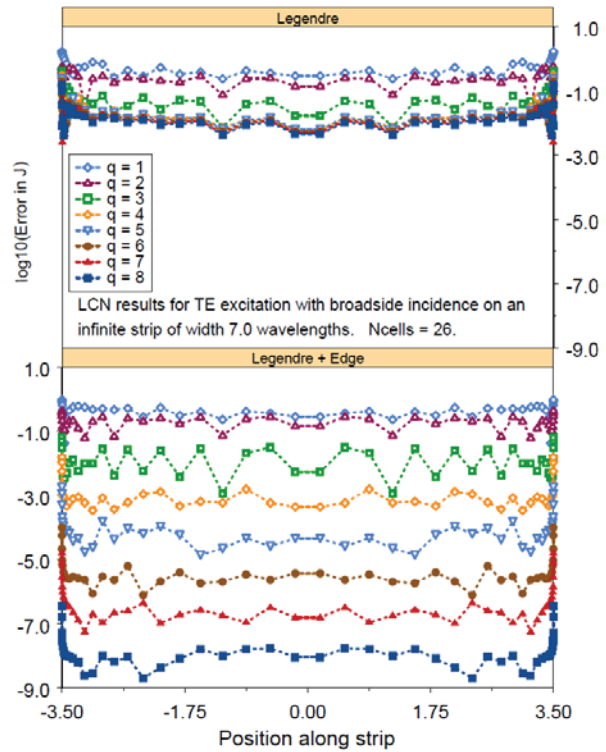


Fig. 5. Error in the TE current density as a function of position and q , for a perfectly conducting 7λ strip illuminated by a normally-incident plane wave. 26 cells are used to model the strip, with the end cells twice as large as the others. The upper figure shows the error when the end cells are treated with the same representation used in other cells; the lower figure shows the error when the singular representation is used in the end cells.

Suppose that each strip of the 3-fin is 7λ in width, and each is divided into cells with the end cells and junction cells twice as large as the others. The same singular representations are used in the end cells as used for the single TE strip in the preceding section; representations in the junction cells are based on terms with exponents in equation (8) from the wedge solution for a 120 degree interior angle. Orthogonal basis functions used for the local corrections for the 120 degree TE case are given by the set in Table II.

In Table II, functions B_1 and B_2 are used for local corrections in cells adjacent to the fin junction for $q = 1$. B_1 through B_4 are used for $q = 2$, etc. Table III presents quadrature rules for implementing the Nyström discretization in the junction cells, assuming $u = 0$ denotes the corner.

Since the 3-fin structure does not have an exact solution, we use the *NRE* to judge the relative accuracy of the results. Figure 6 shows the *NRE* as a function of position along one of the three fins of the structure, for four situations. In the first (upper plot), a conventional nonsingular representation is used in all cells of the model. In the second, a conventional representation is used in all cells except the edge cells, which are treated using a singular representation for a knife edge. In the third, a conventional representation is used in all cells except the junction cells, where the singular representation for a 120 degree wedge is employed. Finally, the fourth case (bottom plot) employs the singular representation for the knife-edge in the edge cells and the singular representation for the 120 degree wedge in the junction cells.

Table II. Basis functions for 120 degrees, TE case.

$$\begin{aligned}
 B_1 &= u^{3/4} \\
 B_2 &= u^{3/4} - \frac{7}{10} \\
 B_3 &= u^{3/4} - \frac{1}{5} - \frac{13}{14} u^{3/2} \\
 B_4 &= u^{3/4} - \frac{1}{26} + \frac{4}{7} u^{3/2} - \frac{99}{65} u \\
 B_5 &= u^{3/4} - \frac{8}{429} + \frac{16}{11} u^{3/2} - \frac{648}{325} u - \frac{2584}{5775} u^{9/4} \\
 B_6 &= u^{3/4} - \frac{5}{528} + \frac{95}{22} u^{3/2} - \frac{1377}{520} u + \frac{323}{105} u^{9/4} - \frac{6561}{1144} u^2
 \end{aligned}$$

From Fig. 6, it is apparent that the overall accuracy does not improve substantially beyond $q = 2$ unless the edge cells employ the singular representation, and that true high order behavior requires that the junction cells also use the enhanced treatment. Figure 7 shows the global *NRE* as a function of the total number of degrees of freedom in the representation, when both edge cells and junction cells employ the singular representations. As in the previous cases, the *NRE* data show increasing slopes with order q and the slopes approximate integer values.

Table III. Weights and nodes associated with the generalized quadrature rule for the TE case, wedge angle = 120 degrees.

nodes	u_i	w_i
2 ($q=1$)	0.13672511222849918533	0.37951320305834680660
	0.72219266699689013444	0.62048679694165319340
4 ($q=2$)	0.01926255761438994475	0.06029440891031772626
	0.16721235939430592191	0.25171152151926467369
	0.51263727731319399021	0.40879441442668019898
6 ($q=3$)	0.88533792190675015565	0.27919965514373740106
	0.00445775138948688208	0.01445955504231629716
	0.04504111963567514576	0.07632091915597698975
	0.17358207080404601792	0.18539035944199733131
	0.41224567448376463466	0.28274134250464589399
	0.70683287748179531992	0.28508835965386458933
	0.93749552578180260021	0.15599946420119889846

At the junction of the 3-fin, the currents flowing into the center point should add to zero, to satisfy Kirchhoff's current law for the TE case. Figure 8 shows the sum of the currents at the center, as a function of degrees of freedom (as the cells are refined) and order q , when both edge cells and junction cells employ the singular representations. From the figure, it is apparent that the satisfaction of KCL improves with increases in both mesh density and in the order q .

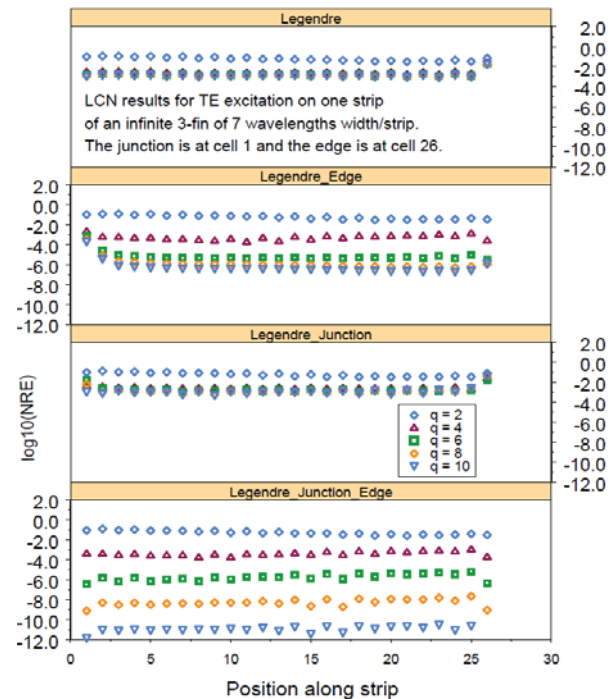


Fig. 6. Local *NRE* results for one fin of the 3-fin structure when illuminated by a TE wave propagating 20 degrees from the x -axis, for four different combinations of representations.

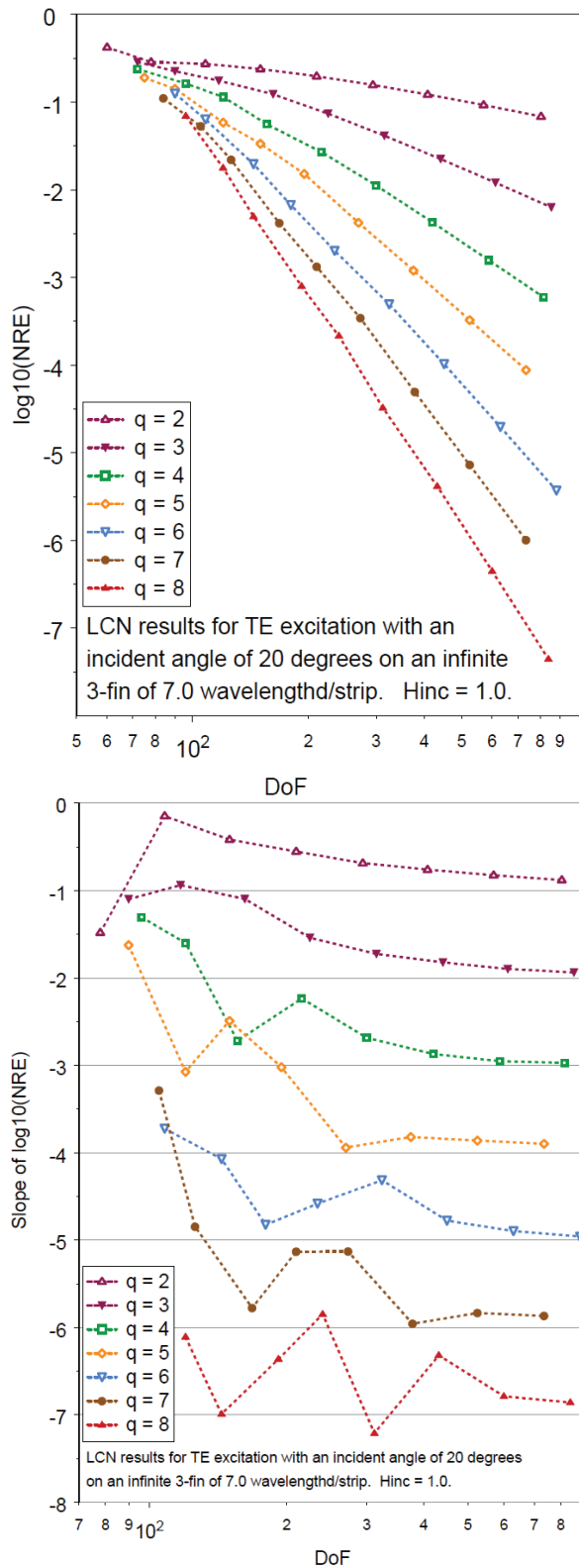


Fig. 7. Global NRE results for the 3-fin when illuminated by a TE wave propagating 20 degrees from the x-axis.

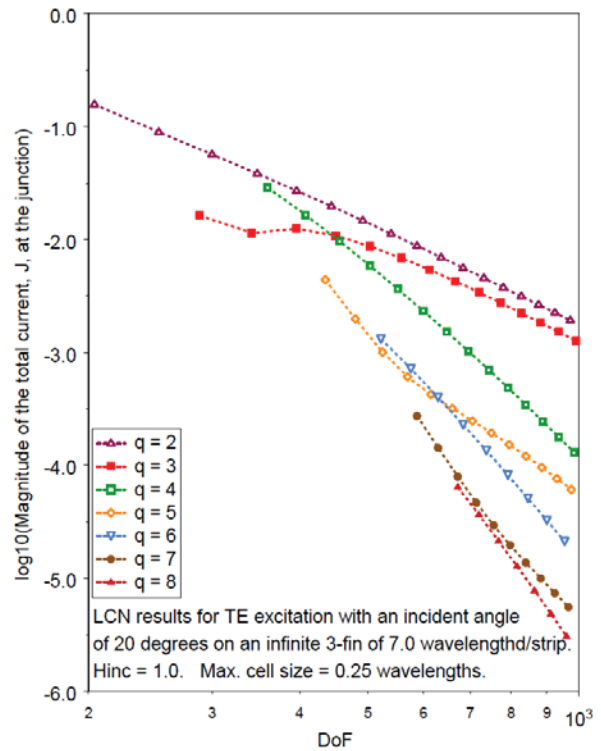


Fig. 8. Sum of the junction currents for the 3-fin, illustrating the extent to which KCL is satisfied as cells are refined for various representation orders q .

In summary, study of the 3-fin structure suggests that junction continuity can be ensured to high order only if the proper junction behavior is incorporated into the representation in the cells at the junction. Treatment using regular cells on either side of a junction will suffice only in the case of two coplanar cells. On the other hand, if it is desired to insulate two cells from each other (an infinitesimal gap), end conditions equivalent to those used at the ends of a TE strip will be required to model that behavior to high order.

VI. EXAMPLE: SCATTERING FROM A HEXAGONAL CONDUCTING CYLINDER

Several examples of the LCN treatment of conducting cylinders with edges are illustrated in [10], including cylinders with triangular and square cross sections. As a final example, we consider the LCN solution of the MFIE for a perfectly conducting hexagonal cylinder, when each face of the cylinder is 3.5λ in width, and a TM wave is incident symmetrically upon one of

the corners between faces. The corners of the hexagon exhibit 120 degree wedge angles, and orthogonal basis functions used for the local corrections for the 120 degree TM case are given by the set in Table IV. In Table IV, functions B_1 and B_2 are used for local corrections for $q = 1$, B_1 through B_4 are used for $q = 2$, etc. Table V presents quadrature rules for implementing the Nyström discretization in the edge cells, assuming $u = 0$ is the corner.

Table IV: Basis functions for 120 degrees, TM case.

$B_1 = u^{-1/4}$
$B_2 = u^{-1/4} - \frac{3}{2}$
$B_3 = u^{-1/4} - 3 + \frac{5}{2}u^{1/2}$
$B_4 = u^{-1/4} - \frac{9}{2} + 10u^{1/2} - 7u$
$B_5 = u^{-1/4} - \frac{216}{35} + \frac{200}{7}u^{1/2} - 72u + \frac{1716}{35}u^{5/4}$
$B_6 = u^{-1/4} - \frac{2187}{280} + \frac{825}{14}u^{1/2} - \frac{1053}{4}u + \frac{1287}{5}u^{5/4} - \frac{187}{4}u^2$

Table V. Weights and nodes associated with the generalized quadrature rule for the TM case, wedge angle = 120 degrees.

nodes	u_i	w_i
2 ($q=1$)	0.06048307438790956835	0.23887432757190171923
	0.63793952019398706980	0.76112567242809828077
4 ($q=2$)	0.00555344256643894865	0.02400445850565570990
	0.103177114071097559074	0.20343338712212968209
	0.43540065702647568767	0.43755946702900373626
	0.86077917841276450835	0.33500268734321087175
6 ($q=3$)	0.00101938730710741485	0.00451930945029498980
	0.02223334550546676504	0.04851941270439041254
	0.12189892349088265974	0.16084006407326768690
	0.34991308210221298855	0.28863159936577654207
	0.66542732067496877426	0.31703773119016205046
	0.92738778900338639928	0.18045188321610831823

Figure 9 shows the global NRE data for this problem, while Fig. 10 shows the NRE as a function of position for various values of order q . On each face of the hexagonal cylinder, the error is relatively uniform, and improves with increasing q . A plot of the magnitude of the current density on three of the six faces of the hexagonal cylinder is shown in Fig. 11.

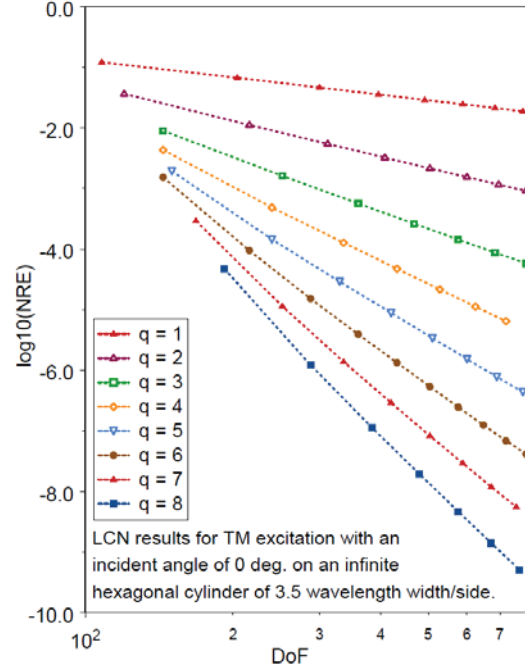


Fig. 9. Global NRE for the hexagonal cylinder, obtained by solving the TM MFIE with LCN.

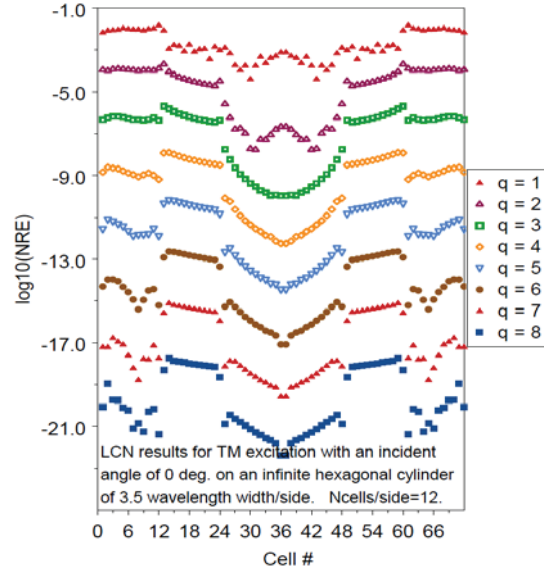


Fig. 10. Local NRE for the hexagonal cylinder example.

VII. CONCLUSIONS

A technique for representing edge and junction effects has been incorporated into the locally-corrected Nyström method. This procedure is shown to produce high order behavior for problems with singularities in the current or charge density at bends or corners. Results having

more than 8 digits of agreement with exact solutions were obtained for the strip examples. Current and charge must also be properly modeled at junctions to maintain high accuracy. For the TE case, where current flows across a junction, as the accuracy of the results improves with representation order the extent to which Kirchhoff's current law is satisfied also improves.

The treatment of more complicated (non-symmetric) junctions remains a topic for future work. It is expected that it may be necessary to incorporate fractional exponents for the full set of wedge angles to properly model the currents in that situation.

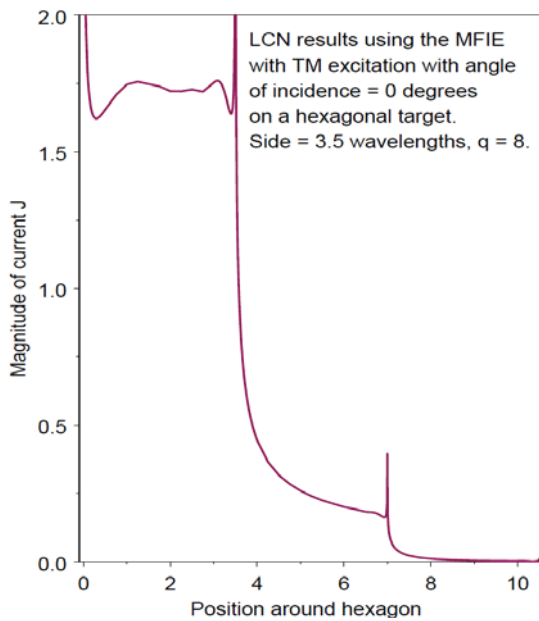


Fig. 11. LCN solution for the current magnitude obtained from the MFIE for a perfectly conducting hexagonal cylinder, when each face of the cylinder is 3.5λ in width, and an TM wave with unit H_z is incident symmetrically upon one of the corners between faces. The solution for $q = 8$ is shown over one half of the computational domain.

APPENDIX A. INTERPOLATION TECHNIQUE USED TO IMPLEMENT IDENTITY OPERATORS WHEN OBSERVATION POINTS DO NOT COINCIDE WITH QUADRATURE NODES

When the observation points coincide with quadrature nodes, the Nyström treatment of

equations such as the MFIE that have an identity-type operator is obvious: the unknown samples become part of the discrete equation. When observation points do not coincide with quadrature nodes, the basis set used to implement local corrections may be used to provide an interpolation. Suppose that the current density $J(u)$ is defined at samples $\{u_1, u_2, \dots, u_p\}$. We seek the coefficients $\{\alpha_i\}$ in the expression

$$J(u_0) = \alpha_1 J(u_1) + \alpha_2 J(u_2) + \dots + \alpha_p J(u_p) = \mathbf{s}^T \begin{bmatrix} \alpha_1 \\ \alpha_2 \\ \mathbf{M} \\ \alpha_p \end{bmatrix} \quad (\text{A.1})$$

where

$$\mathbf{s}^T = \begin{bmatrix} J(u_1) & J(u_2) & \dots & J(u_p) \end{bmatrix}. \quad (\text{A.2})$$

If the samples $\{J(u_i)\}$ are known, we obtain a set of coefficients $\{\beta_i\}$ from the system,

$$\mathbf{M}\mathbf{b} = \begin{bmatrix} B_1(u_1) & B_2(u_1) & \dots & B_p(u_1) \\ B_1(u_2) & B_2(u_2) & & B_p(u_2) \\ \mathbf{M} & & & \mathbf{M} \\ B_1(u_p) & B_2(u_p) & \dots & B_p(u_p) \end{bmatrix} \begin{bmatrix} \beta_1 \\ \beta_2 \\ \mathbf{M} \\ \beta_p \end{bmatrix} = \mathbf{s}, \quad (\text{A.3})$$

where $\{B_i\}$ are the basis functions. The matrix operator \mathbf{M} used on the left-hand side of (A.3) is the same system used in the local correction process for the cell in question [10]. Although the $\{J(u_i)\}$ are not known, in principle we can use the coefficients $\{\beta_i\}$ to determine,

$$J(u_0) = \sum_{i=1}^p \beta_i B_i(u_0) = \mathbf{b}^T \begin{bmatrix} B_1(u_0) \\ B_2(u_0) \\ \vdots \\ B_p(u_0) \end{bmatrix} = \mathbf{s}^T \mathbf{M}^{-T} \begin{bmatrix} B_1(u_0) \\ B_2(u_0) \\ \vdots \\ B_p(u_0) \end{bmatrix} \quad (\text{A.4})$$

where we solved equation (A.3) to obtain $\mathbf{b} = \mathbf{M}^{-1}\mathbf{s}$. By equating (A.1) and (A.4), we obtain the coefficients in equation (A.1) as,

$$\begin{bmatrix} \alpha_1 \\ \alpha_2 \\ \mathbf{M} \\ \alpha_p \end{bmatrix} = \mathbf{M}^{-T} \begin{bmatrix} B_1(u_0) \\ B_2(u_0) \\ \mathbf{M} \\ B_p(u_0) \end{bmatrix}. \quad (\text{A.5})$$

These coefficients $\{\alpha_i\}$ are the weights used to distribute the identity operator among the current density samples when the observation point u_0 is not in the set $\{u_1, u_2, \dots, u_p\}$.

REFERENCES

- [1] L. Canino, J. Ottusch, M. Stalzer, J. Visher, and S. Wandzura, "Numerical solution of the Helmholtz equation in 2D and 3D using a high-order Nyström discretization," *J. Comp. Physics*, vol. 146, pp. 627-663, 1998.
- [2] M. Bibby and A. Peterson, "On the use of over-determined systems in the adaptive numerical solution of integral equations," *IEEE Trans. Antennas Propagat.*, vol. 53, pp. 2267-2273, July 2005.
- [3] E. Klopff, N. Sekeljic, M. Illic, and B. Notaros, "Optimal modeling parameters for higher order MoM-SIE and FEM-MoM electromagnetic simulations," *IEEE Trans. Antennas Propagat.*, vol. 60, pp. 2790-2801, June 2012.
- [4] M. Bibby, A. Peterson, and C. Coldwell, "High order representations for singular currents at corners," *IEEE Trans. Antennas Propagat.*, vol. 56, pp. 2277-2287, August 2008.
- [5] M. Bibby, A. Peterson, and C. Coldwell, "Optimum cell size for high order singular basis functions at geometric corners," *ACES Journal*, vol. 24, pp. 368-374, August 2009.
- [6] S. Gedney, J. Ottusch, P. Petre, J. Visher, and S. Wandzura, "Efficient high order discretization schemes for integral equation methods," *Digest of the 1997 IEEE Antennas and Propagation Society International Symposium*, Montreal, PQ, pp. 1814-1817, July 1997.
- [7] S. Gedney, "Application of the high-order Nyström scheme to the integral equation solution of electromagnetic interaction problems," *Proceedings of the IEEE International Symposium on Electromagnetic Compatibility*, Washington, DC, pp. 289-294, August 2000.
- [8] M. Tong and W. Chew, "Nyström method with edge condition for electromagnetic scattering by 2D open structures," *Progress in Electromagnetic Research*, vol. 62, pp. 49-68, 2006.
- [9] M. Bibby, A. Peterson, and C. Coldwell, "High-order treatment of corner singularities with the locally-corrected Nyström method," *Digest of the 2009 IEEE Antennas and Propagation Society International Symposium*, Charleston, SC, June 2009.
- [10] A. Peterson and M. Bibby, *An Introduction to the Locally-Corrected Nyström Method*, San Rafael: Morgan & Claypool Synthesis Lectures, 2010.
- [11] A. Peterson, M. Bibby, and C. Coldwell, "Satisfaction of end, continuity, and junction conditions by implicit and explicit subsectional Legendre expansions," *Proceedings of the 25th Annual Review of Progress in Applied Computational Electromagnetics*, Monterey, CA, March 2009.
- [12] R. Harrington, *Time Harmonic Electromagnetic Fields*, New York: McGraw-Hill, pp. 238-242, 1961.
- [13] J. Ma, V. Rokhlin, and S. Wandzura, "Generalized Gaussian quadrature rules for systems of arbitrary functions," *SIAM J. Numer. Anal.*, vol. 33, pp. 971-996, June 1996.
- [14] K. Bunch and R. Grow, "Numerical aspects of the boundary residual method," *Int. J. Num. Modelling*, vol. 3, pp. 57-71, 1990.
- [15] K. Bunch and R. Grow, "On the convergence of the method of moments, the boundary-residual method, and the point-matching method with a rigorously convergent formulation of the point matching method," *ACES Journal*, vol. 8, no. 2, pp. 188-202, 1993.
- [16] J. Bowman, T. Senior, and P. Uslenghi, *Electromagnetic and Acoustic Scattering by Simple Shapes*, New York, Hemisphere Publishing, 1987.



Malcolm M. Bibby received the B.Eng. and Ph.D. degrees in Electrical Engineering from the University of Liverpool, in 1962 and 1965, respectively, and an MBA from the University of Chicago. He is currently an Adjunct Professor in ECE at

Georgia Tech. He has been interested in the numerical aspects of antenna design and electromagnetics for more than 30 years.



Andrew F. Peterson received the B.S., M.S., and Ph.D. degrees in Electrical Engineering from the University of Illinois, Urbana-Champaign in 1982, 1983, and 1986 respectively. Since 1989, he has been a member of the faculty of the School of Electrical and

Computer Engineering at the Georgia Institute of Technology, where he is now Professor and Associate Chair for Faculty Development. Within ACES, he has served at various times as a member of the Board of Directors, the Finance Committee Chair, the Publications Committee Chair, and the President. He also served as a technical co-chair for the 25th Annual Review of Progress in Applied Computational Electromagnetics (ACES 2009). He was elevated to ACES Fellow in 2008.